JGR: Biogeosciences

Supporting Information for

Discharge-modulated soil organic carbon export from temperate mountainous headwater streams

Hannah Gies[1], Maarten Lupker[1], Silvan Wick[2], Negar Haghipour[1,3], Björn Buggle[4], Timothy Eglinton[1]

[1] Geological Institute, Department of Earth Sciences, ETH Zürich, Zürich, Switzerland

[2] Soil Science and Biogeochemistry, Department of Geography, University of Zürich, Zürich, Switzerland

[3] Laboratory of Ion Beam Physics, Department of Physics, ETH Zürich, Zürich, Switzerland

[4] Dorfstraße 10, Wennigsen, Germany

Contents of this file

Introduction

We use the average chain lengths (ACL) and the carbon preference index (CPI) of long-chained (> C_{24}) *n*-alkane homologues to delineate sources of organic carbon. In Text S1 we further justify our choice of parameterization.

Text S2 focuses on different possibilities to constrain a vegetation endmember in the studied catchments and explains our choice to differentiate between trees and other vegetation as endmembers in the mixing model.

Figures S1 - S3 and Table S1 supplement the information in Text S1 and S2.

Figure S4 shows the amount of exported carbon in the Erlenbach measured by Smith et al. (2011) in comparison to the data collected in this study

Text S1. Parameterization of Alkane Indices

To use the relative abundance of different long-chain (> C_{24}) *n*-alkane homologues to differentiate between endmembers, the concentrations of the measured *n*-alkanes need to be parameterized.
The chosen indices should comprise as much of the variability of the measured *n*-alkane distribution in the suspended sediments from Erlenbach, Lümpenenbach and Vogelbach as possible. Thus, principal component analysis is used to determine variables that are linear functions of the long-chain *n*-alkane homologues that maximize the explained variance of the long-chain *n*-alkanes in the suspended sediment samples, the so-called principal components (PCs). The Eigenvectors of the two PCs with the highest proportions of explained variance are shown in Table S1.

For PC1 (explained variance: 0.4), the absolute values of most coefficients are similar with values ranging from 0.24 to 0.43. Exceptions are the lower coefficients associated with the *n*-alkanes C_{25} and C_{33}. The direction of the coefficients is opposite for alkanes with odd and even carbon numbers, respectively. The coefficients hence indicate, that a large proportion of the variability of *n*-alkane homologues in the samples can be explained by the relative amount of odd-numbered to even-numbered n-alkanes. An established index, that parameterizes the relative proportion of odd- and even-numbered chain lengths is the carbon preference index (CPI)(equation 1, adapted from Marzi et al. (1993)).

$$CPI = \frac{1}{2}\left(\frac{\sum_{i=n}^{m} C_{2i+1}}{\sum_{i=n}^{m} C_{2i}}\right) + \frac{1}{2}\left(\frac{\sum_{i=n}^{m} C_{2i+1}}{\sum_{i=n+1}^{m+1} C_{2i}}\right) \; with\, n = 12 \; and \; m = 16 \qquad (1)$$

PC2 (explained variance: 0.25) is defined by contrasting directions of the coefficients of shorter-chain (C_{24} – C_{28}) compared to longer-chain (C_{29} – C_{34}) alkanes. This overall distribution of chain lengths is parameterized in the average chain length (ACL)(equation 2, adapted from Poynter and Eglinton (1990)).

$$ACL = \frac{\sum_{i=n}^{m}(2i+1) * C_{2i+1}}{\sum_{i=n}^{m} C_{2i+1}} \; with\, n = 12 \; and \; m = 16 \qquad (2)$$

Figure S1 shows the potential sources of *n*-alkanes and the riverine sediments in the CPI-ACL parameter space.

For purposes of vegetation reconstruction, indices focusing on the C_{27}, C_{29} and C_{31} homologues are used instead of the ACL (e.g., Zhang et al., 2006, Bai et al., 2009, Buggle et al., 2010, Zech et al., 2012). Therefore, an index that only includes C_{27}, C_{29} and C_{31} is also considered as a potential alternative for the ACL (equation 3) to parameterize the relative proportion of shorter versus longer chain lengths.

$$Index_{C_{27}} = \frac{C_{27}}{C_{27} + C_{29} + C_{31}} \qquad (3)$$

The ACL and $Index_{C27}$ of sediment samples and potential endmembers against CPI are shown in Figure S1 and Figure S2, respectively. The $Index_{C27}$ of soil and vegetation endmembers mostly overlap, therefore, the ACL is the better suited parameterization of chain lengths to differentiate between soil and vegetation-derived alkanes in our mixing approach.

Additionally, an index could be used that combines both of the dimensions that best describe *n*-alkane variability in the riverine sediments the proportion of odd compared to even and shorter versus longer chain lengths (equation 4).

$$Index_{combi} = \frac{C_{22} + C_{22}}{C_{27} + C_{29} + C_{31}} \quad (4)$$

As shown in Figure S3, although this combined approach is well suited to differentiate between bedrock-derived *n*-alkanes ($Index_{combi}$ = 1.62 ± 0.1) and biospheric *n*-alkanes ($Index_{combi}$ > 0.3), vegetation- and soil-derived *n*-alkanes cannot be disentangled, rendering this index unsuitable for the mixing approach of this study. CPI and ACL are therefore chosen as parameters for the mixing model, as they enable the best differentiation of endmembers.

Text S2. Constraining the vegetation endmember

The vegetation samples collected in the catchments include the dominant tree species silver fir (*Abies alba*) and Norway spruce (*Picea abies*) as well as green alder (*Alnus viridis*), moss, three different grasses, common rush (*Juncus effusus*), horsetail (*Equisetum*) and ground pines (*Lycopodium*). The distribution of *n*-alkane homologues in the vegetation samples is rather heterogeneous leading to a wide range of potential endmember values with a CPI of 9.1 ± 7.4 and an ACL of 28.1 ± 0.7 (Fig. A1). As four parameters, i.e., $\delta^{13}C$, $\Delta^{14}C$, CPI and ACL, are used for the endmember mixing model, the system of linear equations is fully determined for up to four endmembers, but only three endmembers, namely bedrock, soil and vegetation, are defined. It is therefore possible to divide the vegetation samples into two groups to achieve better constrained endmembers. Silver fir and Norway spruce are the most abundant vegetation in the catchments and therefore potentially dominate the vegetation-derived carbon. Alternatively, moss and green alder grow in the riparian zone, close to the river channels, and could thus be considered as a separate endmember to determine whether their close proximity to the channel is reflected in the river sediments. Finally, grasses could be considered separately to resolve the contribution of grasslands to the exported carbon.

The possible additional vegetation endmembers are shown in Figure S1. Green alder and moss (CPI: 16.6 ± 6.7, ACL: 27.6 ± 0.2) are not a suitable endmember for the model, as ACL and CPI of the riverine sediments are overall significantly closer to the ACL and CPI of the average vegetation endmember compared to the specific green alder and moss endmember. Green alder and moss are also distinct from the other vegetation

samples with respect to $Index_{C27}$ (Fig. S2), a high proportion of the *n*-alkane homologue C_{27} in the riverine sediments could therefore be indicative of most vegetation-sourced organic carbon stemming from vegetation close to the channel. Except for four sediment samples from the Erlenbach catchment and the Lümpenenbach catchment, the sediments feature an $Index_{C27}$ lower than 0.5, therefore green alder and moss do not seem to be dominant sources of *n*-alkanes to the sediment despite their proximity to the channel.

The distribution of *n*-alkane homologues in the grass samples collected in the catchments is rather heterogenous, leading to significant variability in CPI (12.2 ± 5.3) and ACL (28.4 ± 0.8) values. The range of the grass endmember is therefore similar to the overall vegetation and does not tighten quantitative constraints on contributions. Silver fir and Norway spruce are similar in their *n*-alkane signal (CPI, 4.4 ± 1.4; ACL, 27.8 ± 0.3). Additionally, their *n*-alkane signatures, with a comparably low ACL and CPI, is also observable in river sediments (Fig. S1). Therefore, the most abundant tree species are separated from the other vegetation as an additional endmember.

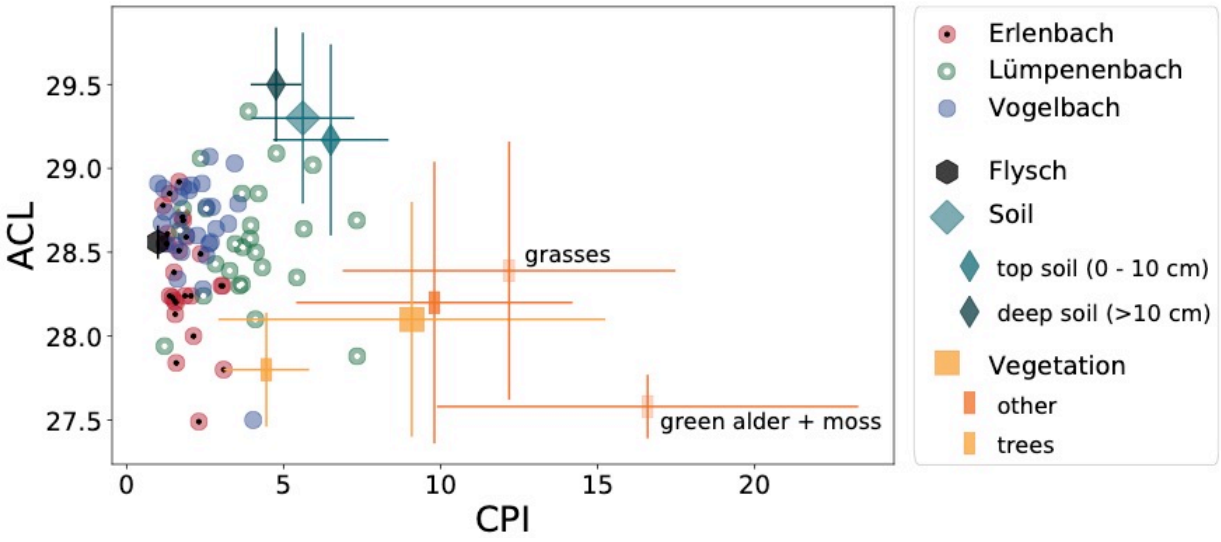

Figure S1. ACL of sediment samples and potential endmembers plotted against CPI

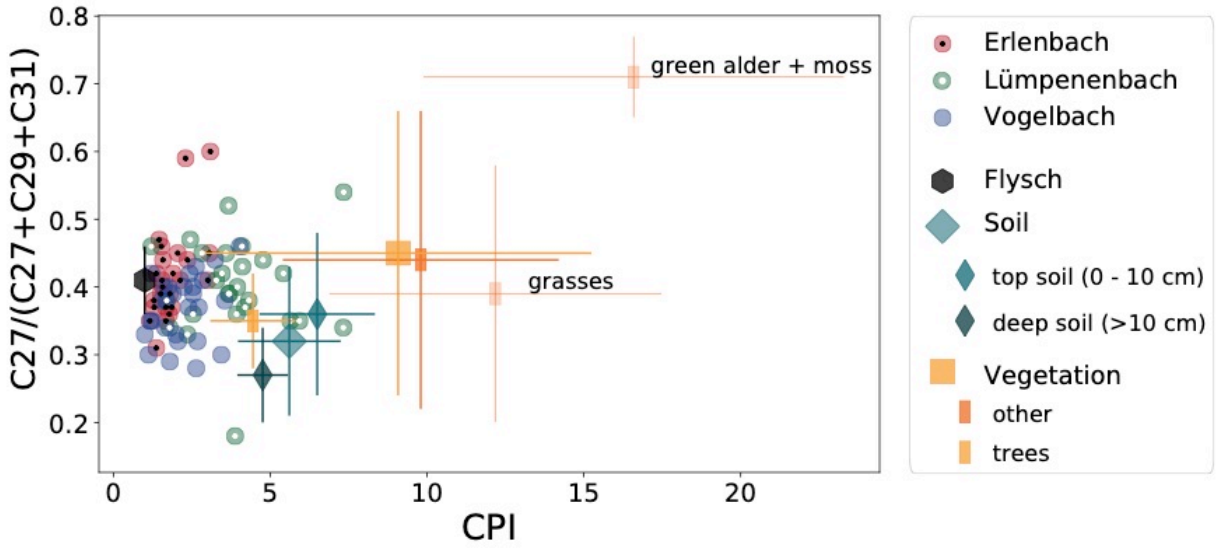

Figure S2. C27/(C27 + C29 + C31) of sediment samples and potential endmembers plotted against CPI.

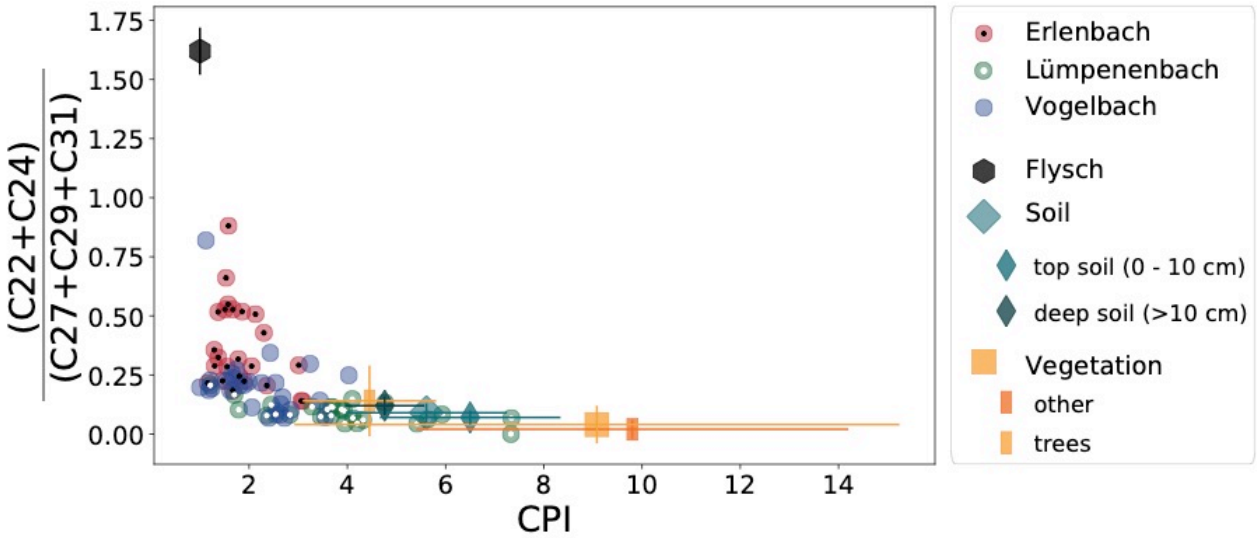

Figure S3. The ratio of short-chain (< C26) even-numbered to long-chain odd-numbered homologues of sediment samples and potential endmembers plotted against the CPI. This index combination is suited to differentiate between bedrock-derived and biospheric n-alkanes, while vegetation- and soil-derived n-alkanes are not discernable.

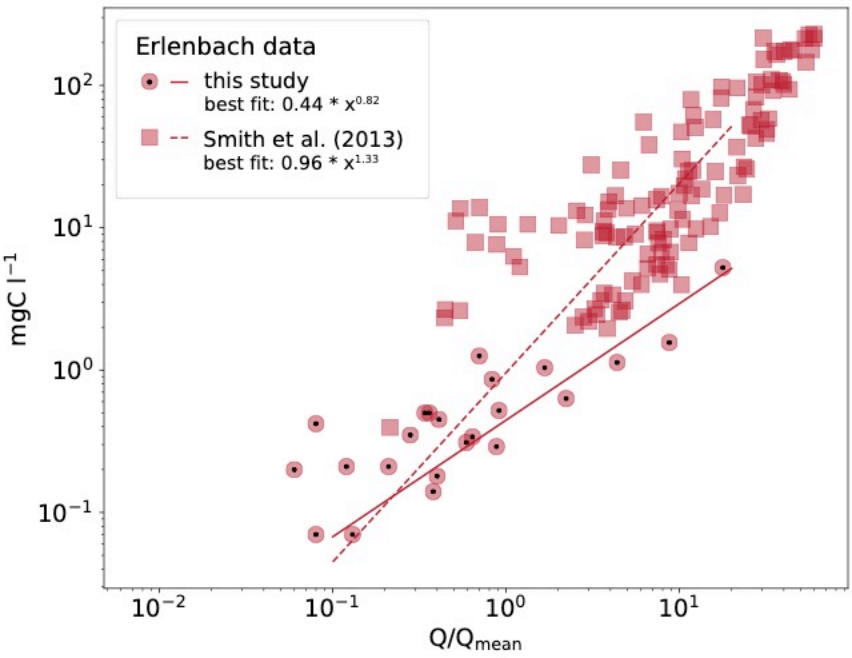

Figure S4. Organic carbon concentration of the suspended sediment collectedin the Erlenbach catchment in this study compared to Smith et al. (2013). The OC concentrations measured in this study are consistently lower compared to the concentrations measured by Smith et al. (2013) resulting in different power-laws

***n*-Alkane homologue**	**PC1 (0.40)**	**PC2 (0.25)**
C_{24}	-0.29	0.34
C_{25}	0.00	0.52
C_{26}	-0.39	0.23
C_{27}	0.36	0.21
C_{28}	-0.34	0.05
C_{29}	0.43	-0.07
C_{30}	-0.32	-0.31
C_{31}	0.30	-0.26
C_{32}	-0.27	-0.27
C_{33}	0.06	-0.38
C_{34}	-0.24	-0.35

Table S1. Eigenvectors of the first two principal components of the long-chained *n*-alkane distribution in river sediments. The variance explained by the PCs is given in brackets. The magnitude and direction of the coefficients of the original variables, i.e. the concentration of *n*-alkanes with carbon numbers between 24 and 34, indicate the influence of the respective alkane homologue for the PC.

References

Bai, Y., Fang, X., Nie, J., Wang, Y., & Wu, F. (2009). A preliminary reconstruction of the paleoecological and paleoclimatic history of the Chinese Loess Plateau from the application of biomarkers. *Palaeogeography, Palaeoclimatology, Palaeoecology*, *271*(1-2), 161-169.

Buggle, B., Wiesenberg, G. L., & Glaser, B. (2010). Is there a possibility to correct fossil n-alkane data for postsedimentary alteration effects?. *Applied Geochemistry*, *25*(7), 947-957.

Marzi, R., Torkelson, B. E., & Olson, R. K. (1993). A revised carbon preference index. *Organic Geochemistry*, *20*(8), 1303-1306.

Poynter, J., & Eglinton, G. (1990). 14. Molecular composition of three sediments from hole 717c: The Bengal fan. In *Proceedings of the Ocean Drilling Program: Scientific results* (Vol. 116, pp. 155-161).

Smith, J. C., Galy, A., Hovius, N., Tye, A. M., Turowski, J. M., & Schleppi, P. (2013). Runoff-driven export of particulate organic carbon from soil in temperate forested uplands. *Earth and Planetary Science Letters*, 365, 198-208.

Zech, M., Rass, S., Buggle, B., Löscher, M., & Zöller, L. (2012). Reconstruction of the late Quaternary paleoenvironments of the Nussloch loess paleosol sequence, Germany, using n-alkane biomarkers. *Quaternary Research*, *78*(2), 226-235.

Zhang, Z., Zhao, M., Eglinton, G., Lu, H., & Huang, C. Y. (2006). Leaf wax lipids as paleovegetational and paleoenvironmental proxies for the Chinese Loess Plateau over the last 170 kyr. *Quaternary Science Reviews*, *25*(5-6), 575-594.